

A Simplified Physical Foundation

The Lorentz-Invariant Universe Resulting from Two Constraints

David B. Schmitz

Quantum Wavespace Theory Project (QWST)

December 30, 2025

Abstract

We present a simplified physical foundation based on only two constraints: a finite propagation speed C and an energy density saturation threshold P_0 . Together these constraints define a Lorentz-invariant wavespace substrate in which nonlinear compression is dynamically redistributed through saturated eigenmode geometry. Under sustained energy influx, this redistribution enforces global standing-wave organization across both nonlinear and linear regimes. The simultaneous enforcement of these constraints establishes a global resonant scale R_0 and a microscopic saturation scale r_0 , imposing a discrete spectrum of stable eigenmodes.

Two fundamental geometric families emerge within this constrained substrate: a saturated spherical reservoir and a cylindrical or toroidal transport channel. Their interaction yields two independent coupling invariants, identified with the fine-structure constant α and the Rydberg constant R_∞ . In this framework, mass, charge, and coupling strengths arise as emergent features of boundary geometry and mode structure rather than as fundamental inputs. Infinitesimal boundary leakage at the global scale couples back to local modes, producing a persistent attractive effect identifiable with gravitation in the weak-field limit.

Established physical theories are recovered as effective descriptions of these constrained geometric dynamics within their respective domains of validity. The framework is not constructed by fitting numerical values to known constants, but as a closed physical system whose eigenmode structure yields dimensionless couplings and scale relations as natural outcomes of the underlying constraints. As such, it offers a physically grounded starting point with the potential to clarify longstanding conceptual gaps and unexplained relationships in fundamental physics.

Contents

1 A Simplified Physical Foundation	4
The universe is modeled as a continuous wavespace substrate governed by two universal limits—a causal propagation speed C and a saturation bound P_0 —from which all admissible standing-wave behavior follows.	
2 A Universe Constrained by Causality C and Saturation P_0	4
Whenever curvature attempts to exceed the admissible limit P_0 , it is redirected outward at speed C , enforcing a steep-gradient boundary and preventing runaway collapse in the medium.	
3 Steep-Gradient Saturation Defines the Quantization Scale r_0	5
Saturation produces a flat interior compression region bounded by a single steep-gradient shell at r_0 , beyond which the profile relaxes into the oscillatory return ladder of the truncated spherical eigenmode.	
4 The Global Standing-Wave Cavity Emerges	6
An initially oversaturated medium drives a nonlinear saturation front outward until a closed recurrence becomes possible at R_0 , thereby establishing the universe's self-selected standing-wave cavity.	
5 Eigenmodes Arise at the Critical Scale Ratio R_0/r_0	7
The coexistence of a microscopic saturation scale r_0 and a cosmic recurrence scale R_0 enforces discrete radial structure, fixing the geometric ratios that determine all allowed eigenmodes of the medium.	
6 Boundary Leakage Maintains Coherence and Stabilizes the Global Mode	8
Perfect reflection cannot maintain phase coherence across the global cavity; an infinitesimal boundary leakage removes non-recurrent components and stabilizes the single coherent global eigenmode.	
7 Two Irreducible Internal Geometries Survive	9
Only two internal geometries survive the (C, P_0) constraint: saturated spherical j_0 modes that store energy, and cylindrical/toroidal J_0 modes that redirect steepening laterally without forming a saturation wall.	
8 The Spherical Eigenmode Establishes Energy and Mass	10
The saturated spherical mode possesses a fixed intrinsic energy determined entirely by its curvature-weighted profile, establishing the microscopic energy scale from which nucleon mass emerges.	
9 The Planck Action Scale Set by C and P_0	11
The saturation and causality limits jointly imply a natural action scale linking microscopic curvature to macroscopic recurrence, forming a geometric bridge between P_0 , r_0 , and the observed value of $\hbar C$.	
10 Geometric Superposition Determines the Coupling Constants	12
Two geometric overlap channels—sphere-sphere coupling g_Σ and sphere-cylinder coupling k_Σ —govern all coherent interactions between internal modes and fix the structure of atomic and electromagnetic behavior.	
11 Physical Constants Follow Directly from the Geometric Hierarchy	16

Fundamental constants such as α , R_∞ , and the nucleon–electron mass ratio arise directly from the geometric couplings and standing-wave structure imposed by the (C, P_0) constraints.

12 Gravity Emerges from Boundary Leakage	18
The minute inward shift $\delta r_0/r_0$ required to maintain global coherence induces a refractive potential $\Phi \simeq C^2(\delta r_0/r_0)$, yielding Newtonian gravity and a geometric expression for G .	
13 Convergence of GR, SR, QM, and the Standard Model	20
The standing-wave substrate defined by (C, P_0) reproduces the essential structures of GR, SR, QM, and the Standard Model as symmetry projections of a single geometric operator, offering a unified and predictive foundation for fundamental physics.	
A Equivalent Physical Forms of the Universal Operator	22
B Fundamental Constraints and Parameters	23
C Sphere–Cylinder Return Ladder and k_Σ	24
D Sphere–Sphere Coupling and the Rydberg Constraint	27
E Additional Static-Field Relations	30
F Derivation of Gravity from Leakage at R_0	30

List of Tables

1	Dependencies of fundamental mass and energy constants	12
2	Core Constants with Coupling Dependencies	17
3	Equivalent representations of the universal operator	22
4	Fundamental Values of the Standing–wave System	23
5	QWST Predictions Compared with CODATA	23

1 A Simplified Physical Foundation

Conventional field theories permit arbitrarily large gradients and unbounded local energy density, admitting solutions that are mathematically consistent but physically pathological. We instead begin from the minimal requirements that any real medium must obey: a finite propagation speed C and a finite maximum sustainable energy density P_0 .

The causal limit C alone is insufficient to render standing-wave dynamics well posed. If energy density were unbounded, arbitrarily steep gradients could form within arbitrarily short times, allowing the action of a mode to diverge even in a causally limited medium. A saturation bound is therefore required to enforce finite action. Together, the limits (C, P_0) ensure that neither temporal response nor spatial compression can diverge, forcing excess drive to be redistributed geometrically rather than accumulated locally.

These two constraints are sufficient to generate a finite resonant cavity with well-defined geometric scales. Standing-wave solutions must self-organize so as to respect both limits everywhere, giving rise to bounded eigenmodes whose characteristic lengths, energies, and recurrence times are fixed by the geometry of the saturated region. This minimal starting point provides the foundation for the structures that later manifest as relativistic, quantum, and electromagnetic behavior.

The framework introduced here defines Quantum Wavespace Theory (QWST). Rather than modifying quantum field theory or general relativity, QWST provides a geometric substrate from which their characteristic constants and interaction scales emerge in the appropriate limits. It therefore serves as a unifying eigenmode picture: not superseding established physics, but explaining why its fundamental parameters take the values observed.

2 A Universe Constrained by Causality C and Saturation P_0

The causal limit C restricts the rate at which information and phase may propagate, while the saturation limit P_0 bounds the maximum admissible local gradient. When an excitation approaches this bound, further compression cannot be supported; excess drive is redirected outward at speed C . This self-adjusting response prevents runaway steepening and forces the formation of a region in which the waveform reaches its maximum allowable gradient. The transition from a saturated interior to a relaxed exterior defines a natural geometric boundary within the medium.

A minimal representation of the substrate is therefore given by the propagation law

$$\partial_t \psi = C \mathcal{L}[\psi],$$

together with the saturation condition

$$|\nabla \psi| = P_0 \quad (\text{at the boundary}).$$

Definition. The field $\psi(r, t)$ denotes the scalar standing-wave profile of the substrate, representing the local amplitude of compression and phase displacement at radial distance r . The admissible-gradient constraint $|\nabla \psi| \leq P_0$ enforces a saturated interior region whose geometry determines the allowed eigenmodes, the stored energy, and the interaction scales derived in subsequent sections.

Several parallel forms of the universal operator \mathcal{L} are summarized in the Appendix, Table 3, including its relativistic, Lagrangian, and quantum-mechanical forms, together with other physically equivalent representations. These formulations make explicit that the same underlying dynamics reproduce the familiar structures of relativistic wave theory, Hamiltonian/Lagrangian mechanics, quantum evolution, optical index variation, and the weak-field metric of general relativity.

For present purposes we focus on the symmetry properties of \mathcal{L} : under spherical symmetry and the (C, P_0) saturation limits, the mode that minimizes the maximal gradient is the saturated j_0 profile, which therefore determines the nucleon’s interior geometry.

The combined constraints enforce the emergence of both a global radius and a microscopic saturation scale.

Use of Term Curvature. Throughout this document, the term “curvature” refers exclusively to *steep-gradient curvature of the mode profile*, not spacetime curvature in the sense of general relativity. It denotes the local steepness of the standing-wave profile as it approaches the saturation bound set by P_0 —the quantity that governs the gradient energy of the mode and must remain below the admissible slope imposed by the medium.

3 Steep-Gradient Saturation Defines the Quantization Scale r_0

Whenever the wavefield attempts to concentrate energy faster than the medium can respond, the radial profile sharpens until the local curvature reaches the saturation limit set by P_0 . Beyond this point the medium cannot sustain further compression, and the steepest region collapses into a thin saturated layer located at a definite radius.

This mechanism defines the microscopic scale r_0 :

- it is the radius at which the curvature first attains the maximum admissible gradient, and
- beyond which additional steepening is prohibited by the nonlinear limit of the medium.

Because saturation is a purely local process determined only by (C, P_0) , the radius r_0 forms essentially instantaneously during any high-compression event. It is not determined by atomic physics or later structure; it is the geometric footprint of the medium’s nonlinear limit.

During formation, excess energy continues to push outward whenever a region attempts to exceed P_0 , enforcing the saturation constraint and redistributing curvature throughout the standing wave.

When local gradients reach the saturation bound P_0 , the waveform enters a nonlinear regime in which regions of pinned gradient form. These saturated regions organize into layered structures within the standing wave, producing a piecewise eigenmode distinct from the smooth j_0 profile of the unsaturated limit. As additional energy is supplied, the number and extent of these layers increase, but the structures themselves persist as stable components of the globally coherent eigenmode. Global coherence does not eliminate these layers, but rather fixes their geometry and phase relationships within the saturated eigenmode.

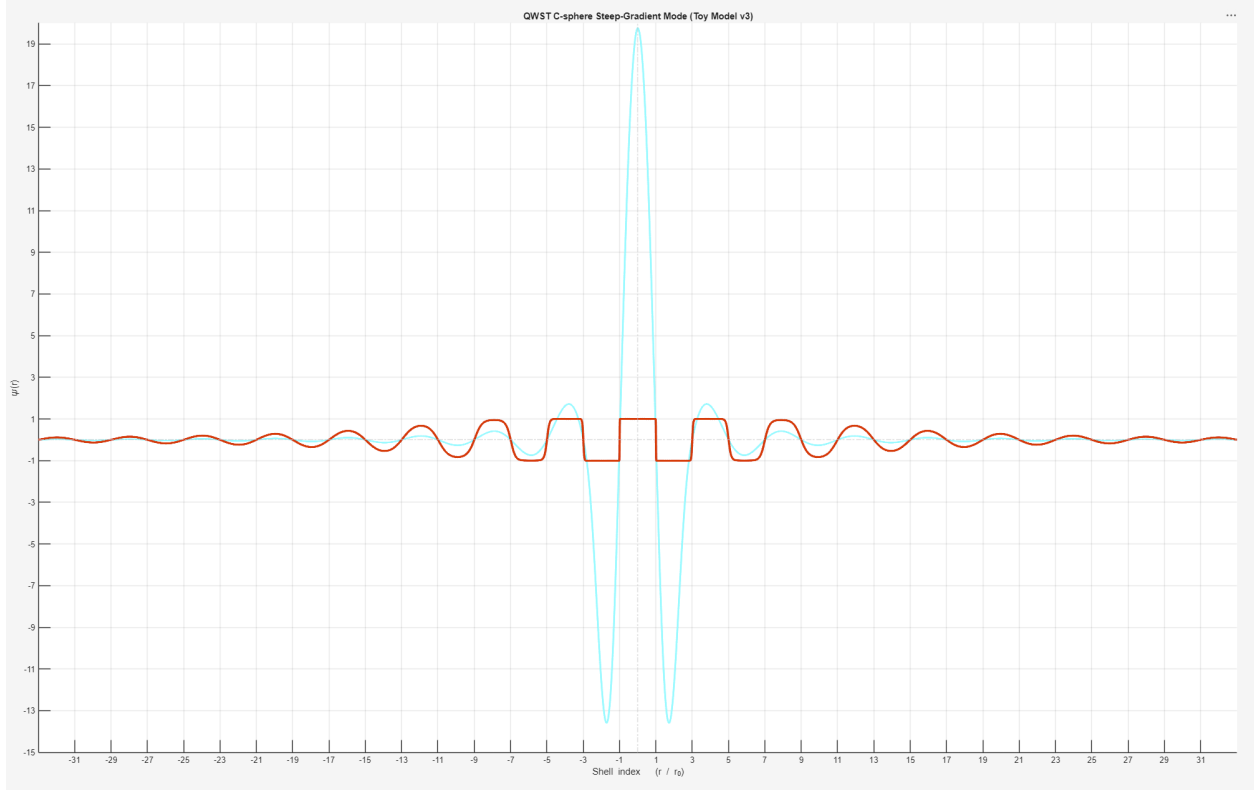


Figure 1: Illustrative 1D toy model comparing the linear spherical Bessel mode j_0 (cyan) with a saturation-limited profile (red) obtained by enforcing a global pressure cap $|\psi| \leq P_0$ while keeping the total energy fixed. This plot illustrates how a steep-gradient boundary and flat-topped saturation layer naturally emerge when a maximum admissible pressure is enforced, and does not represent the full 3D eigenmode. This saturation mechanism generates the microscopic scale r_0 and the corresponding geometric return gain g_Σ coupling.

Uniqueness of the saturated spherical mode. Once the pressure profile reaches the admissible gradient imposed by P_0 , the only spherically symmetric standing wave that satisfies both (i) a fixed microscopic node at r_0 and (ii) a monotonic decrease of curvature toward the exterior is the saturated representative of the j_0 family. Any attempt to construct a different radial profile with the same node would either violate the maximal slope allowed by P_0 or introduce additional interior nodes that destroy global coherence. Thus the saturated j_0 profile is not an ansatz but the *unique* spherical mode compatible with both (C, P_0) and the steep-gradient boundary. Because saturation is enforced locally whenever $|\nabla\psi|$ reaches its maximum admissible value, the radius r_0 is selected essentially instantaneously: no global coordination is required to form the steep-gradient boundary.

Boundary leakage progressively removes all components that fail to return in phase across the entire cavity. Only the coherent spherical eigenmode survives this filtering, leaving a single stable standing-wave structure anchored at the radius r_0 defined by saturation.

4 The Global Standing-Wave Cavity Emerges

Once the microscopic saturation layer at r_0 forms, additional compression no longer steepens the profile but instead drives energy outward. Unlike r_0 , which is fixed locally by saturation, the outer radius R_0 is a relaxation scale: it is determined by how far the outward-moving saturation fronts

can propagate before the pressure curvature falls below the threshold set by P_0 . Each time the medium attempts to exceed P_0 , a new steep layer is triggered, and this adjustment propagates radially away from the core. The outward cascade continues until the pressure profile relaxes to a radius where the field no longer approaches saturation.

That radius is the *self-selected* global boundary R_0 : the smallest radius at which the outward propagation of saturation ceases and a stable return flow becomes possible. Uniqueness follows because each outward saturation adjustment decreases the profile curvature monotonically; once the gradient falls below the admissible threshold, no further saturated layers can form. No external scale is imposed; R_0 emerges solely from the interaction of the wave speed C , the saturation threshold P_0 , and the need for the outward adjustment to reinject coherently. The saturation front propagates outward until the curvature of the profile falls below the steep-gradient threshold, at which point no further layers can form. Beyond this radius the returning field remains within the linear regime and can rejoin the core in phase. Thus R_0 is the unique radius at which saturation ceases and a closed, causally consistent recurrence cycle first becomes possible.

The microscopic and macroscopic radii therefore arise from the *same* physical limitation, expressed at vastly different scales:

$$r_0 \text{ from local saturation,} \quad R_0 \text{ from global relaxation.}$$

Once P_0 is fixed, both radii follow; there is no freedom to choose an independent cavity size. Together they define the two ends of the cosmic cavity,

$$r_0 \ll R_0,$$

with r_0 set essentially immediately by steep-gradient saturation and R_0 determined by large-scale relaxation under (C, P_0) .

5 Eigenmodes Arise at the Critical Scale Ratio R_0/r_0

Once the saturated geometry has stabilized, the cavity is constrained by only two immutable geometric conditions:

1. a fixed microscopic node at r_0 imposed by the steep-gradient saturation limit, and
2. a fixed global phase condition at R_0 required for coherent boundary leakage and reinjection.

These two radii completely determine the allowed standing-wave structure. A global wave can persist only if each round trip returns to the core with the same phase. Because leakage enforces phase matching, the wavelength of the surviving mode is forced into the unique value that simultaneously satisfies both the microscopic and macroscopic constraints. Any pattern that fails this test is gradually removed by boundary leakage.

A note on cosmological interpretation. The purpose of this section is not to reproduce the full Einstein field equations or the Friedmann system, but to show that the leading-order gravitational and cosmological behavior of the saturated cavity is consistent with the weak-field and large-scale limits of general relativity.

Although R_0 acts as a fixed geometric boundary for the coherent eigenmode, this does not conflict with the observed Hubble expansion [35]. A slow leakage-induced contraction of the internal wavelength is observationally indistinguishable from a metric expansion, because redshift measurements depend only on the ratio $\lambda_{\text{obs}}/\lambda_{\text{emit}}$. Thus a constant R_0 and a shrinking internal

wavelength reproduce the standard distance–redshift relation without modifying any cosmological data. In this sense the redshift is a bookkeeping of phase slippage rather than spatial expansion: a shorter internal wavelength at the moment of emission produces the same observational signature as an expanding geometry. Because all inferred cosmological distances depend only on the accumulated redshift, a shrinking internal wavelength reproduces the standard luminosity–distance and angular–diameter relations without modifying the observational phenomenology.

The smallest admissible half-wavelength is approximately

$$\lambda_{\min} \simeq 2r_0,$$

while the cavity scale sets the largest allowed wavelength. Their ratio defines the dimensionless *capacity number*

$$N = \frac{R_0}{r_0},$$

which counts how many fundamental wavelengths can fit between the two boundaries.

When N is small, only trivial oscillations satisfy the boundary conditions. When N is large, the cavity supports a hierarchy of long-lived internal modes, including the spherical and cylindrical components responsible for the observed coupling constants discussed below. In this sense, once (C, P_0) fix the ratio R_0/r_0 , they also fix the entire spectrum of admissible eigenmodes.

The microscopic radius r_0 changes only at the level of $\delta r_0/r_0 \sim 10^{-43}$ per cycle due to leakage back-reaction (Eq. 30). Thus r_0 is effectively fixed from the moment saturation is first reached, while R_0 is set by macroscopic relaxation. Quantization of the global geometry is therefore not an extra assumption but a direct consequence of combining saturation at r_0 with phase closure at R_0 .

6 Boundary Leakage Maintains Coherence and Stabilizes the Global Mode

A perfectly reflecting boundary at R_0 cannot maintain coherent global oscillation. Any microscopic timing or amplitude mismatch would accumulate with each round trip, preventing the system from settling into a unique eigenmode; a perfectly closed cavity admits an enormous family of nearly degenerate patterns with no mechanism to select one. As established in cavity optics [27], perfectly reflecting boundaries are unstable under phase mismatch and necessarily admit a small transmissive channel.

The medium therefore stabilizes itself through an infinitesimal but essential leakage at R_0 : a negligible fraction of the mode escapes each cycle, removing precisely those components that fail to reproduce themselves after one global recurrence. This leakage acts as a coherence filter, eliminating all non-recurring patterns while leaving the true eigenmode strictly undamped.

Leakage as coherence selection, not dissipation. The infinitesimal transmissivity of the boundary at R_0 does not act as a dissipative loss mechanism. The escaping component is precisely the portion of the field that fails to reproduce itself after one global round trip; the coherent component is recaptured exactly and reinjected. Thus leakage performs the same role as out-coupling in optical resonators: it eliminates non-eigenmodes while leaving the true eigenmode strictly undamped. Stability of the global standing wave therefore follows from selective filtering, not energy decay.

Crucially, leakage-driven adjustment occurs coherently across the entire cavity. Once the phase of the global mode is fixed by recurrence at R_0 , every radius must share the same wavelength; no region can sustain an independent local scale. Non-coherent nonlinear features that fail to reproduce

after a global recurrence are gradually removed, while saturation layers that close coherently are preserved as part of the eigenmode.

Localized internal structures that *do* reproduce themselves after each cycle are preserved as part of the eigenmode content; everything else is exported through the boundary. Stabilization is therefore not a separate postulate but the unavoidable outcome of combining a fixed cavity (r_0, R_0) with a boundary that leaks just enough to discriminate between coherent and non-coherent patterns.

7 Two Irreducible Internal Geometries Survive

Although a saturated medium could in principle support many eigenmodes, the constraints (C, P_0) collapse all admissible excitations to two geometric archetypes. This structural reduction under strong geometric limits is not unique to the present framework. In Ricci flow, Perelman showed that regions of high curvature evolve generically into spherical caps and cylindrical necks [12, 13]. In Loop Quantum Gravity, gauge-invariant excitations reduce to 0-dimensional nodes and 1-dimensional links [15, 14]. Across these very different theories, imposing strong geometric constraints leaves only two stable spatial modes.

Two saturation-compatible geometries. Under the (C, P_0) constraints, only two internal geometries remain stable:

- (i) **Spherical modes (j_0 family).** These provide isotropic compression reservoirs that minimize gradient energy and store the largest amount of energy per unit radius. They form the baryonic sector: protons, neutrons, nuclear shells, and any saturated quasi-pointlike excitation. The steep-gradient layer associated with approaching the P_0 limit occurs in spherical modes because excess curvature must compress radially, forcing the formation of a saturated shell.

Among spherically symmetric modes subject to the admissible-gradient constraint $|\nabla\psi| \leq P_0$, the saturated j_0 profile provides the lowest-gradient solution and the only one that can sustain a coherent return ladder. It is therefore the physically admissible spherical mode under the (C, P_0) constraints.

- (ii) **Cylindrical modes (J_0 family).** These redistribute gradient along an axis, supporting circulation and long-range phase transport. They form the leptonic and radiative sector: electrons, photons, neutrinos, and quark transport channels. Unlike spherical modes, which have no alternative path for excess curvature, a cylindrical (or toroidal) mode can redirect approaching steep gradients into azimuthal circulation around the axis. This lateral redistribution prevents the formation of a radial saturation shell even when the local slope approaches the P_0 bound, allowing the cylindrical mode to remain admissible without generating a return ladder.

Why only two geometries survive the saturation limit. The bound P_0 restricts the admissible gradient of ψ in every direction. Spherical j_0 modes distribute curvature isotropically and therefore minimize the maximal slope; cylindrical J_0 modes distribute curvature axially and likewise avoid any local concentration that would exceed P_0 . Higher multipoles are excluded because their angular nodes concentrate curvature into shrinking sectors, forcing $|\nabla\psi|$ above the saturation limit. Thus the (C, P_0) constraints admit exactly two internally stable families: an isotropic spherical reservoir and an axial cylindrical transport channel.

Saturation resolved through geometric redirection. Both geometries are subject to the same steep-gradient limit, but they satisfy it in different ways. A spherical j_0 mode has no lateral path for excess curvature, so any attempt to exceed the admissible slope forces the formation of a steep boundary at r_0 and a corresponding spherical return ladder. A cylindrical mode, by contrast, redirects the approaching steep gradient into azimuthal circulation around the axis. This lateral redistribution relieves radial pressure before a steep wall can form, allowing the cylindrical mode to remain sub-saturated *without* creating a spherical boundary or a geometric return ladder. Thus the electron satisfies the same (C, P_0) limit as the nucleon, but resolves it through curvature redirection rather than spherical confinement.

Global cavity mode. Independent of particle excitations, the medium supports a single global standing-wave envelope spanning $0 < r < R_0$. This background mode is not a particle; its saturated profile defines the microscopic radius r_0 , the global radius R_0 , and the reference wavelength that sets the scale for all internal modes.

Lowest-order particle modes. Within the two archetypes, the lowest-gradient excitations are:

1. **The nucleon:** a saturated j_0 spherical mode confined by the boundary at r_0 , serving as the fundamental energy reservoir. Only here does a steep-gradient interior layer appear.
2. **The electron:** a minimal-gradient cylindrical mode derived from a J_0 profile, supporting axial circulation and providing the long-range electromagnetic channel. This excitation remains entirely below the admissible slope.

These two eigenmodes supply the geometric basis for the dimensionless couplings (α, g_Σ) that govern atomic structure. All higher excitations are composite or higher-order realizations of these two archetypes, scaled and constrained by the global cavity mode.

8 The Spherical Eigenmode Establishes Energy and Mass

With the geometric structure fixed, the intrinsic energies of the saturated modes follow directly from their curvature-weighted profiles. The saturated cavity supports a fundamental spherical eigenmode whose energetic content is set entirely by the limits (C, P_0) and the microscopic radius r_0 . This mode furnishes the geometric energy scale used throughout the subsequent derivations of physical constants.

Spherical-Mode Energy

At maximum compression the saturated spherical eigenmode stores energy in the form of a bounded, non-radiative energy density $P(r)$ limited by the saturation scale P_0 and confined within the steep-gradient boundary at radius r_0 . The total energy associated with the spherical mode is obtained by integrating this energy density over the volume of the C-sphere,

$$E_n \equiv \int_0^{r_0} P(r) 4\pi r^2 dr,$$

where $P(r) \leq P_0$ represents the saturation-limited stored energy density of the wavespace substrate. Evaluating this integral for the saturated spherical profile yields the total *mode energy* of the nucleon,

$$E_n = \frac{3}{2} A P_0 r_0^3, \tag{1}$$

where the purely geometric factor is

$$A \equiv \frac{16(\pi^2 - 8)}{3\pi^2}.$$

Confined Core Energy and Rest Mass

The mode energy E_n represents the full reversible oscillatory energy budget of the spherical eigenmode and includes contributions from three equivalent axial exchange channels. Only a fraction of this energy corresponds to energy that is permanently confined within the saturated core and therefore contributes to the invariant rest mass of the nucleon. We define the confined core energy E_c as the non-radiative energy stored within the saturated C-sphere,

$$E_c \equiv A P_0 r_0^3. \quad (2)$$

The relation between the mode energy and the confined core energy follows from the decomposition of the spherical mode into three equivalent axial exchange channels, each carrying a half-cycle exchange energy. This yields

$$E_n = \frac{3}{2} E_c, \quad (3)$$

or equivalently,

$$E_c = \frac{2}{3} E_n. \quad (4)$$

Since the confined core energy E_c is non-radiative and represents the invariant energy of a stationary spherical eigenmode, the nucleon rest mass follows directly from the relativistic energy relation,

$$m_n = \frac{E_c}{C^2} = \frac{A P_0 r_0^3}{C^2}. \quad (5)$$

This mass is therefore an intrinsic property of the saturated spherical mode and requires no coupling to other degrees of freedom; it establishes the fundamental energy scale against which cylindrical and toroidal interaction modes are later defined.

9 The Planck Action Scale Set by C and P_0

Action is the product of energy and time. In an unconstrained medium, either factor may be taken arbitrarily large, allowing the action of a mode to diverge. In a wavespace substrate subject simultaneously to a maximum admissible energy density P_0 and a maximum propagation speed C , neither energy nor time can increase without bound. The coexistence of these two limits therefore enforces a finite and universal action scale.

The saturation constraint P_0 bounds the maximum energy that can be stored within a localized region of the substrate, while the causal limit C bounds the minimum time required for information or phase to propagate across that region. Once a spherical eigenmode reaches saturation at radius r_0 , additional drive cannot further increase the spatial gradient; instead, excess input is redirected into temporal phase advance. As a result, spatial compression and temporal frequency become kinematically linked.

The characteristic action associated with a saturated exchange across the C-sphere is obtained by combining the confined core energy with the minimum traversal time set by the causal limit. The confined (non-radiative) core energy of the saturated spherical mode is

$$E_c = A P_0 r_0^3,$$

and the minimum time required for phase or energy to traverse the saturated core diameter is

$$\tau = \frac{2r_0}{C}.$$

The resulting action scale is therefore

$$\mathcal{A} = E_c \tau = A P_0 r_0^3 \left(\frac{2r_0}{C} \right). \quad (6)$$

Multiplying by C gives the invariant combination

$$\mathcal{A} C = A P_0 r_0^3 (2r_0), \quad (7)$$

which is identified with the observed quantity $\hbar C$.

In this sense, Planck's constant does not enter as an independent postulate, but as the finite action required to complete a minimal saturated exchange cycle in a (C, P_0) -limited medium.

Once this geometric action scale is established, the familiar quantum relation

$$E = \hbar \omega$$

emerges as a bookkeeping identity relating energy to phase advance per unit time. Here \hbar appears as the universal conversion factor between frequency and energy precisely because the underlying wavespace enforces a fixed quantum of action.

In summary, the saturation limit P_0 prevents unbounded spatial compression, while the causal limit C prevents arbitrarily rapid temporal response. Their coexistence enforces a finite action scale, making the appearance of Planck's constant an unavoidable consequence of the (C, P_0) constraints rather than an independent axiom.

The relations of Sections 8 and 9 are summarized in Table 1, which collects the dependencies of the fundamental mass and energy constants on the universal limits (C, P_0) and the spherical cosine integral $A \equiv 16(\pi^2 - 8)/3\pi^2$.

Table 1: Dependencies of fundamental mass and energy constants on (C, P_0) and spherical cosine integral A . All quantities in this table are expressed in standard SI units.

Description	Symbol =	Limits	Geometry
<i>nucleon mass</i>	$m_n C^2 =$	P_0	$r_0^3 A$
<i>nucleon mode energy</i>	$E_n =$	P_0	$r_0^3 A (3/2)$
<i>Planck (bridge form)</i>	$\hbar C =$	P_0	$r_0^3 A (2 r_0)$

10 Geometric Superposition Determines the Coupling Constants

A saturated nucleon possesses only two irreducible internal geometries: (i) the isotropic j_0 reservoir defined by the steep-gradient boundary at r_0 , and (ii) the axial cylindrical mode that provides the transport channel associated with the electron. All admissible interactions must therefore arise

from how these two geometries superpose and communicate within the standing-wave substrate. No additional independent modes exist: the (C, P_0) constraints collapse the interaction space to this minimal two-mode basis.

Why only two couplings can exist. Because the j_0 reservoir contains two symmetric spherical branches and the cylindrical mode provides a single axial sampling direction, the medium admits exactly two distinct and nonredundant ways for energy to be exchanged:

1. *Sphere-sphere coupling* (g_Σ): coherent exchange between the two spherical branches of the saturated j_0 reservoir. This channel measures how efficiently the nucleon can redirect inward-returning flux from one hemisphere to the other.
2. *Sphere-cylinder coupling* (k_Σ): geometric sampling of the spherical return by the axial cylindrical mode. This channel determines how the nucleon communicates with the electron's transport geometry and sets the strength of long-range electromagnetic behavior.

These are the only couplings the medium can support. A cylindrical mode alone never reaches the saturation gradient P_0 and therefore cannot form its own focusing boundary or return ladder; without such a structure no new gain factor can appear. Thus a cylinder-cylinder interaction introduces no independent dimensionless constant: macroscopically it reduces to the same electromagnetic channel already encoded in k_Σ and expressed through α .

Minimal three-mode Hamiltonian. In the basis of the two spherical branches and the axial cylindrical mode, the uncoupled energies form the diagonal of

$$H_0 = \begin{pmatrix} E_n & 0 & 0 \\ 0 & E_n & 0 \\ 0 & 0 & E_e \end{pmatrix},$$

where E_n is the saturated energy contained within the C-sphere and E_e is the reduced energy of the cylindrical mode. In the absence of coupling, the spherical branches each store the saturated energy E_n associated with the j_0 reservoir. The cylindrical mode, however, does not experience the full spherical drive: its energy is reduced by the purely geometric projection of the spherical pressure field onto the axial aperture. The direct integration of this projection (Appendix C) yields the factor

$$B \equiv \frac{2(\pi - 2)}{\pi^2 - 8},$$

so that the intrinsic energy of the uncoupled cylindrical mode is

$$E_e = B E_n.$$

Thus B encodes the geometric mismatch between isotropic storage and axial transport, and uniquely determines the baseline energy of the cylindrical mode. This reduction is therefore not an assumption or normalization, but the geometric consequence of sampling the spherical return through a single axial channel. (Appendix C).

Coherent superposition introduces the two geometrically allowed couplings:

$$H = \begin{pmatrix} E_n & g_\Sigma & k_\Sigma \\ g_\Sigma & E_n & k_\Sigma \\ k_\Sigma & k_\Sigma & B E_n \end{pmatrix}.$$

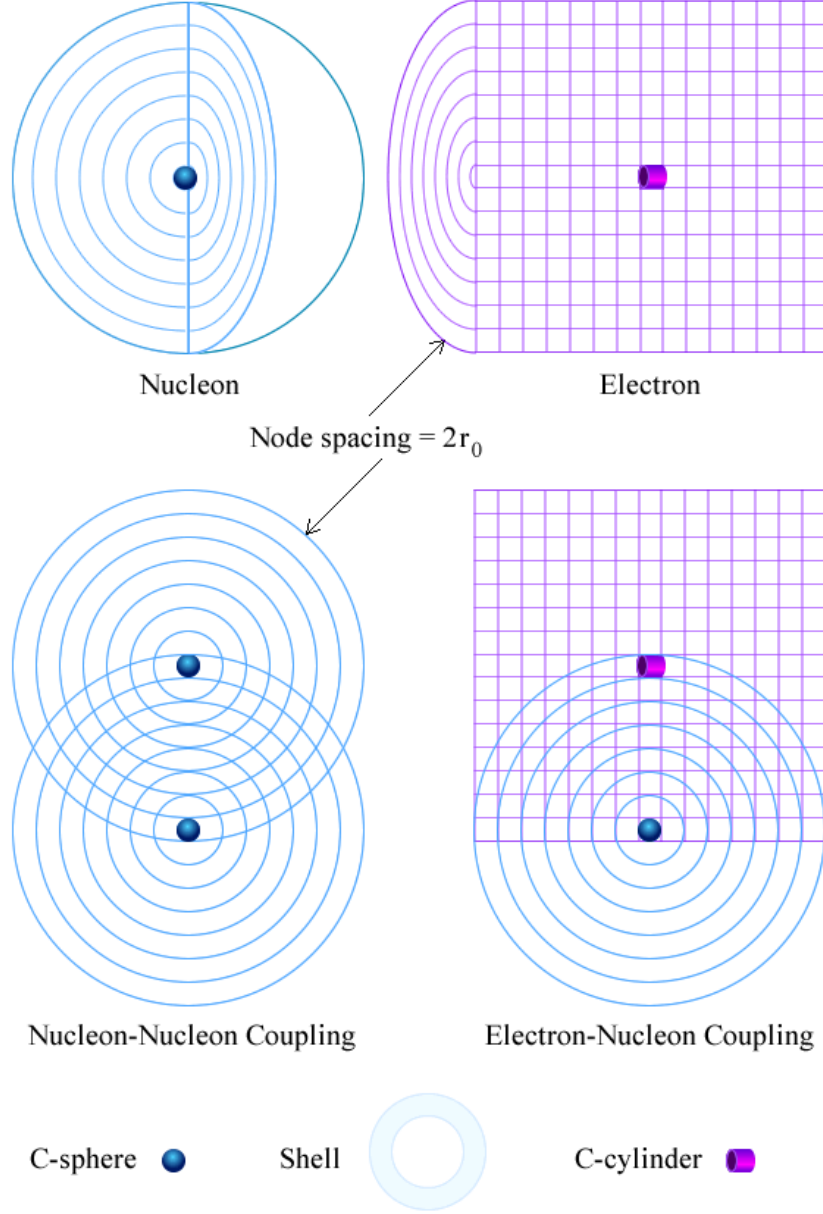


Figure 2: Spherical and cylindrical saturation geometries. Left: the nucleon's saturated j_0 profile with node spacing $2r_0$. Right: the electron's minimal-gradient cylindrical mode. Bottom panels illustrate geometric overlap: nucleon–nucleon coupling is set by the projected disc area πr_0^2 of each C–sphere, while nucleon–electron coupling samples the same projected area but through a single axial cylindrical channel.

The geometric couplings g_Σ and k_Σ appear as the off-diagonal overlap integrals of the reduced three-mode Hamiltonian for the spherical and cylindrical standing-wave branches. These integrals encode the coherent exchange between the two spherical submodes and the axial sampling of the spherical return, respectively.

The coupling structure is fixed by symmetry: the two spherical branches are related by reflection and therefore share a single mutual exchange channel g_Σ , while the axial mode admits only one independent overlap with the spherical reservoir, giving k_Σ . All higher-order sphere-cylinder or cylinder-cylinder mixings vanish by symmetry, leaving exactly two geometric couplings in the three-mode basis.

At this level of description, the full interaction structure of the nucleon-electron system is encoded entirely in the two dimensionless geometric constants g_Σ and k_Σ . Once these are fixed by the saturated geometry of the standing-wave medium, no additional freedom remains: the fine-structure constant, static charge, electron mass, and the long-range form of electromagnetic interaction follow directly from this three-mode eigensystem.

Sphere-Cylinder Coupling k_Σ

The cylindrical mode samples only the axial (radial-projection) component of the nucleon's spherical return field. This sampling factor is fixed entirely by geometry and contains no adjustable freedom.

Geometric origin of the spherical eigenvalue 98. The saturated j_0 reservoir generates a hierarchy of outward-return contributions. Each round trip contributes a geometrically weighted amplitude proportional to $N^{-2}2^{-N}$, and summing over all such returns yields the exact spherical ladder eigenvalue

$$k_\Sigma^{(\text{sph})} = 96 + 2 = 98,$$

as derived in Appendix C. This value is a pure geometric invariant of the saturated C-sphere and is not a fitted parameter.

Axial projection of the spherical return. A cylindrical mode does not intercept the full isotropic field; it receives only the RMS axial fraction of the spherical return,

$$\langle \cos^2 \theta \rangle_\Omega = \frac{1}{\sqrt{3}},$$

which represents the geometric projection of an isotropic field onto a single axis.

Total sphere-cylinder gain. Combining the spherical ladder eigenvalue with the axial projection gives

$$k_\Sigma = k_\Sigma^{(\text{sph})} + \frac{1}{\sqrt{3}} = 98 + \frac{1}{\sqrt{3}} = 98.5773502692 \dots$$

The integer 98 reflects the full saturated spherical return capacity, while the additive $1/\sqrt{3}$ arises solely from the axial geometry of cylindrical sampling.

Connection to the fine-structure constant. With k_Σ fixed, the dimensionless fine-structure constant follows directly from the two-mode Hamiltonian:

$$\alpha^{-1} = \frac{16}{3\pi B} k_\Sigma, \tag{8}$$

with the projection factor B and the return-ladder value k_Σ .

Sphere–Sphere Coupling g_Σ

The second constant g_Σ characterizes the coherent return capacity of the nucleon itself. It is determined experimentally by the Rydberg constant R_∞ . The sphere–sphere coupling g_Σ is controlled by the remaining coherent return of the proton at the ionization threshold. The sphere–sphere coupling g_Σ is determined by the projected area πr_0^2 of the saturated C–sphere, not the full $4\pi r_0^2$ surface.

The Rydberg constant R_∞ measures this limit directly: at R_∞ , the spherical return allocated to the electron channel is maximized and the reservoir is depleted. This yields the geometric relation

$$g_\Sigma^2 = \frac{1}{144 r_0 R_\infty}, \quad (9)$$

with full derivation in Appendix D.

Using the theoretical value of r_0 and the CODATA value of R_∞ we find the approximate value of g_Σ

$$g_\Sigma \approx 978.673468 \dots,$$

Therefore small perturbations are magnified $\approx 10^3$ giving rise to the Coulomb barrier, and amplifying the infinitesimal leakage from the cavity boundary at R_0 . The full derivation is given in Appendix D.

Implications. With B , k_Σ , and g_Σ fixed by the geometry of the standing–wave substrate, all electromagnetic quantities follow from the structure of the Hamiltonian. The fine–structure constant, static charge, and electron mass emerge as direct consequences of the two couplings, with no free parameters introduced at any stage. These relationships are summarized in Section 11 Table 2.

11 Physical Constants Follow Directly from the Geometric Hierarchy

With the geometric origins of the coupling constants established, we extend our relationship table to include electron mass, static charge, Bohr radius and ionization energy. All quantities in this table follow from the two geometric couplings (g_Σ, k_Σ) and the saturation scale (P_0, r_0) ; no value listed here is an independent parameter.

Table 2: Dependencies of the core constants on the saturation scale P_0 , the fine structure constant α , the Rydberg constant R_∞ , and the geometry of the C -sphere.

Description	Constant	P_0	α	R_∞	Geometry
<i>nucleon mass</i>	$m_n C^2$	$= P_0$	—	—	Ar_0^3
<i>nucleon mode energy</i>	E_n	$= P_0$	—	—	$Ar_0^3 (3/2)$
<i>Planck bridge</i>	hC	$= P_0$	—	—	$Ar_0^3 (2r_0)$
<i>static charge</i>	e^2	$= P_0$	α	—	$Ar_0^3 (4r_0) \varepsilon_0$
<i>electron mass</i>	$m_e C^2$	$= P_0$	α^{-2}	R_∞	$Ar_0^3 (4r_0)$
<i>ionization energy</i>	E_I	$= P_0$	—	R_∞	$Ar_0^3 (2r_0)$
<i>Bohr radius</i>	a_0	$=$	α	R_∞^{-1}	$1/4\pi$

Note: All electromagnetic quantities are expressed in SI; the geometric relations are unchanged by unit conventions. Converting e^2 from CGS to SI requires the factor $4\pi\varepsilon_0 = 10^7/C^2$ (with $\mu_0\varepsilon_0 = 1/C^2$; $\mu_0 = 4\pi \times 10^{-7}$).

Consistency of Coupling Constants and the Dimensionless Mass Ratio

An important relationship arises from the ratio of the masses of the nucleon and electron

$$\frac{m_n}{m_e} = \frac{\alpha^2}{4r_0 R_\infty}.$$

Solving for r_0 gives the following result

$$r_0 = \frac{\alpha^2 m_e}{4m_n R_\infty}.$$

Inserting the CODATA values for $(\alpha, R_\infty, m_p/m_e)$ gives

$$r_0 = 6.6070492769 \times 10^{-16} \text{ m},$$

thus, the nucleon radius can be determined using measured values (α, R_∞) .

Conceptual significance. This relation is not a numerical coincidence but an expression of the fact that three ostensibly unrelated constants of nature,

$$\alpha, \quad R_\infty, \quad \frac{m_n}{m_e},$$

all encode the *same* geometric return gain of the saturated spherical mode. The electron mass suppression, the hydrogenic binding scale, and the nucleon core radius are therefore not independent physical inputs: they are three projections of a single piece of geometry. Once the saturated mode fixes r_0 , the same return gain g_Σ necessarily produces both the observed fine-structure constant and the neutron-electron mass ratio. In this sense the microscopic scale of nuclear structure, the scale of atomic binding, and the electron mass hierarchy arise from one irreducible geometric mechanism, leaving no adjustable freedom in the coupling structure of the theory.

Parameter-Free Determination of the Nucleon Scale

The two independent roles of the sphere–sphere coupling g_Σ may be combined to eliminate it entirely. From the two–mode Hamiltonian, the proton–electron mass ratio obeys

$$\frac{m_n}{m_e} = (6g_\Sigma\alpha)^2,$$

while the Rydberg constant fixes the same coupling through the sphere–sphere return gain,

$$R_\infty = \frac{1}{16N_r^2 r_0} = \frac{1}{144g_\Sigma^2 r_0}.$$

Eliminating g_Σ yields the purely dimensionless relation

$$\frac{m_n}{m_e} = \frac{\alpha^2}{4r_0 R_\infty},$$

so that the nucleon radius is determined directly by measured quantities,

$$r_0 = \frac{\alpha^2 m_e}{4m_n R_\infty}.$$

It is worth noting that the radius r_0 identified above coincides with a familiar relativistic length scale. Using the Planck bridge relation $hC = m_n C^2 (2r_0)$, one finds

$$2r_0 = \frac{h}{m_n C},$$

which is precisely the Compton wavelength of the proton. Thus the saturated core diameter emerges as the proton Compton wavelength, providing a consistency check on the geometric interpretation of the C-sphere scale.

No QWST–specific parameter enters this expression: r_0 is fixed entirely by $\{\alpha, R_\infty, m_e, m_n\}$. Once r_0 is known, the core pressure P_0 and the return gain g_Σ follow from

$$m_n = \frac{AP_0 r_0^3}{C^2}, \quad g_\Sigma = \frac{1}{6\alpha} \sqrt{\frac{m_n}{m_e}},$$

closing the system with no remaining freedom.

12 Gravity Emerges from Boundary Leakage

Gravity does not participate in the formation of the cosmic cavity. The universe first relaxes into its unique global standing–wave eigenmode determined by the limits (C, P_0) . Only *after* this coherent mode is established does gravity emerge.

Once the global mode exists, the outer boundary at R_0 must maintain phase coherence from one recurrence to the next. A perfectly reflecting boundary cannot accomplish this: any microscopic timing or amplitude mismatch would accumulate indefinitely. As in optical resonators, a boundary with infinitesimal transmissivity is required to remove non-recurrent components.

This leakage forces a tiny inward adjustment of the saturated core radius. Let δr_0 denote the microscopic inward shift of r_0 needed to restore phase matching after one round-trip of the global wave. It is important to emphasize that leakage does not dissipate the global mode: the coherent

component is re-injected exactly, while only the non-recurrent components are lost. Thus leakage serves as a selection mechanism for the eigenmode rather than an energy sink.

Although δr_0 is extraordinarily small, it is coherent across the entire cavity and therefore produces a systematic wavelength deficit in regions containing additional nucleons. The leakage-induced change in the local recurrence time produces a fractional wavelength shift

$$\frac{\delta\lambda}{\lambda} \propto \frac{\delta r_0}{r_0},$$

and therefore an effective refractive potential

$$\Phi \simeq C^2 \frac{\delta r_0}{r_0}.$$

This is exactly the weak-field potential appearing in geometric optics and the Newtonian limit of general relativity.

Newton's constant G emerges as

$$G = g_\Sigma \frac{E_n}{r_0^2 m_n^2} \delta r_0. \quad (10)$$

The incremental leakage is (see Appendix F):

$$\frac{\delta r_0}{r_0} = \frac{9}{16\pi} \frac{r_0}{R_0}, \quad (11)$$

This contraction is enormously suppressed by the cosmic ratio r_0/R_0 . With representative values $r_0 \simeq 6.6 \times 10^{-16}$ m and $R_0 \simeq 1.3 \times 10^{26}$ m, Eq. (11) gives

$$\delta r_0 \approx (9 \times 10^{-43}) r_0 \approx 6 \times 10^{-58} \text{ m}.$$

Although negligible at the scale of individual particles, this microscopic lag is multiplied by the coupling gain g_Σ and summed over enormous numbers of interacting nucleons. The result is the macroscopic gravitational force described by G .

Formation of an index gradient. Because δr_0 is coherent but the amplification is localized, the global cavity cannot accommodate the same wavelength everywhere. Instead the medium forms a slowly varying refractive index field,

$$n(\mathbf{x}) = 1 - \frac{\Phi(\mathbf{x})}{C^2},$$

whose gradient compensates for the leakage-driven adjustment. Where nucleons cluster, the effective wavelength is slightly shorter, and the index n is slightly larger. The global mode adjusts so that the phase accumulated around any closed loop remains constant. This is the origin of the gravitational potential Φ . The refractive index field is not imposed externally but is generated self-consistently by the leakage deficit of the saturated j_0 mode. Maintaining constant phase accumulation over closed paths forces a unique curvature of the global mode, leading directly to the Newtonian potential.

Interpretation. The chain of causation may be viewed as a refractive process: boundary leakage \rightarrow microscopic shift $\delta r_0 \rightarrow$ wavelength deficit \rightarrow spatial index gradient \rightarrow macroscopic acceleration. Gravity therefore reflects the curvature of the global mode's phase field, not a separate force introduced into the system.

Weak-field limit. A test particle or wavepacket moves according to the spatial variation of the local phase velocity C/n . Expanding $n = 1 - \Phi/C^2$ gives

$$\frac{d^2\mathbf{x}}{dt^2} = -\nabla\Phi,$$

the Newtonian equation of motion. Thus the inverse-square force between two masses arises directly from the spatial redistribution of the leakage-driven wavelength deficit. The magnitude of Φ depends only on δr_0 and the sphere-sphere gain factor g_Σ ; no additional fields are required.

Strong-field behavior. In regions where many nucleons contribute coherently, the index gradient steepens and the phase velocity decreases. Light rays bend because their trajectories follow gradients of C/n . Frequencies redshift because the proper recurrence period lengthens as n increases.

The “horizon” of a gravitationally bound object occurs at the radius where the local recurrence cycle of the standing wave slows to the point that it can no longer outpace the leakage-induced phase deficit. Beyond this point the mode cannot complete a coherent inward-return cycle, and the global phase accumulates at the minimal rate allowed by boundary stabilization. At this point the standing-wave cycle cannot shorten further, and the global mode accumulates phase at the slowest rate allowed by boundary stabilization. This mirrors the GR description in which the proper time of an infalling observer dilates to zero at the horizon.

At this radius the mode becomes marginally compressible, and the resulting refractive-index profile reproduces the strong-field signatures of general relativity, including gravitational redshift, Shapiro delay, and lensing. A full strong-field treatment, including the contraction metric and horizon structure, is given in the complete QWST framework [35].

Interpretation. Gravity emerges as the macroscopic imprint of boundary stabilization rather than as a separate interaction. The same leakage δr_0 that stabilizes the global standing wave produces a coherent wavelength deficit that is amplified at nucleons and distributed through the medium as a refractive index gradient. Once (C, P_0) fix r_0 and R_0 , and the sphere-sphere gain is set by R_∞ , the weak-field gravitational interaction follows with no additional assumptions.

13 Convergence of GR, SR, QM, and the Standard Model

Beginning only with the two universal limits (C, P_0) , the medium is forced into a finite resonant cavity whose microscopic saturation scale r_0 and global radius R_0 emerge self-consistently from the standing-wave dynamics. Within this cavity we find:

- (i) two fundamental geometric families (a saturated spherical reservoir and a cylindrical/toroidal transport channel),
- (ii) two independent geometric couplings (g_Σ, k_Σ) that fix the long-range nucleon-electron and electromagnetic behavior at leading order,
- (iii) a single mechanism—boundary leakage—that produces gravitational refraction and recovers the Newtonian/GR limits with no additional fields.

The constants of nature therefore arise not as adjustable inputs but as *geometric consequences* of a saturated, Lorentz-invariant standing-wave medium. Once the cavity forms and infinitesimal leakage selects the coherent global mode, the admissible excitations, their interactions, and the numerical values of the associated constants are no longer free to vary.

This stands in contrast to frameworks that assume unbounded curvature, unbounded compression, or arbitrarily localizable energy—assumptions that may simply not hold in nature. Imposing the two limits (C, P_0) removes these idealizations and replaces them with a structure that is stable, divergence-free, and automatically quantized.

Once (C, P_0) restrict the admissible geometry and enforce saturation plus leakage, the resulting standing-wave system offers no remaining adjustable freedom: the particle spectrum, the coupling constants, and gravity itself emerge as unavoidable consequences of the two fundamental limits.

APPENDIX

A Equivalent Physical Forms of the Universal Operator

The universal operator introduced in Sections 1–3 admits several equivalent representations depending on which symmetry, limit, or coordinate frame is emphasized. These forms—relativistic, quantum-mechanical, optical, and metric—do not represent independent physical assumptions. They are all reductions of the same standing-wave relation $\partial_t \Psi = C \mathcal{L}[\Psi]$ when projected onto different subspaces of the eigensystem. In particular, the familiar Schrödinger operator, the covariant energy–momentum relation, and the weak-field gravitational metric arise as distinct slow-wave limits of this single geometric operator. Table 3 summarizes these correspondences.

Table 3: Equivalent forms of the universal operator \mathcal{L} in established physical frameworks.

Framework / Interpretation	Mathematical Expression
Universal operator form — abstract standing-wave relation defining the medium	$\partial_t \Psi = C \mathcal{L}[\Psi], \quad \nabla \Psi = P_0 \text{ at boundary}$
Relativistic wave form — represents the general standing-wave field in spacetime	$\frac{1}{C^2} \frac{\partial^2 \Psi}{\partial t^2} - \nabla^2 \Psi + k_0^2 \Psi = 0$
Lagrangian (action–principle) form — yields the universal standing-wave equation incorporates the steep–gradient saturation as a constraint	$\mathcal{L} = \frac{1}{2}(\partial_t \Psi)^2 - \frac{C^2}{2} \nabla \Psi ^2 - V_{\text{sat}}(\nabla \Psi)$ $V_{\text{sat}}(\nabla \Psi) \rightarrow \infty \quad \text{for } \nabla \Psi > P_0$
Quantum–mechanical form — yields the Schrödinger equation in the slow-wave (non-relativistic) limit	$\hat{H} \Psi = E \Psi, \quad \hat{H} = -\frac{\hbar^2}{2m} \nabla^2 + V(r)$
Invariant energy–momentum form — expresses the same relation in manifestly covariant form	$\hat{P}^\mu \hat{P}_\mu \Psi = \frac{E^2}{C^2} - \mathbf{p}^2 = m^2 C^2$
Refractive index (lensing equivalence) — reproduces the first-order variation of wave velocity and optical index directly from the global standing-wave eigenmode	$\frac{\delta C}{C} = -\frac{\delta r_0}{r_0}, \quad n(x) \simeq 1 - \frac{\Phi(x)}{C^2}$
Metric correspondence — shows that the same relation reproduces Einstein’s weak-field metric coefficients	$g_{00} \simeq 1 + \frac{2\Phi}{C^2}, \quad g_{rr} \simeq -\left(1 - \frac{2\Phi}{C^2}\right)$

Each of these is a reduction or slow-wave limit of the same universal operator when projected into the appropriate coordinate frame or symmetry group. These parallel forms illustrate that the universal operator of Section 1.3 naturally subsumes the familiar equations of quantum mechanics,

relativity, and field theory— and even reproduces Einstein’s gravitational lensing directly from the standing-wave geometry of the global cavity.

B Fundamental Constraints and Parameters

Table 4: Fundamental Geometric Parameters of the Standing-wave System. These three scales (r_0, R_0, P_0) arise directly from the limits (C, P_0) and define the global and microscopic structure of the Lorentz-invariant, pressure-bounded standing-wave cavity. R_0 corresponds to the Hubble Distance ($D_H \approx 1.300 \times 10^{26}$).

Quantity	Symbol	Value
C-sphere radius	r_0	$6.6070492769 \times 10^{-16}$ m
Macroscopic boundary radius	R_0	$1.289799105690940 \times 10^{26}$ m
Maximum pressure	P_0	$5.159027571213943 \times 10^{35}$ Pa
Speed of light (reference)	C	$2.99792458000 \times 10^8$ m/s
Geometric factor (spherical weighting)	$A \equiv 16(\pi^2 - 8)/(3\pi^2)$	1.0102961646
Geometric projection factor	$B \equiv 2(\pi - 2)/(\pi^2 - 8)$	1.2213055761
Sphere-sphere coupling (dimensionless)	g_Σ	978.673468079993768
Sphere-cylinder coupling (dimensionless)	k_Σ	98.577350269

Table 5: Key physical constants predicted by the geometric standing-wave system defined by the limits (C, P_0). All quantities below the first divider are *parameter-free predictions*, computed solely from the relations among (r_0, P_0, g_Σ) and compared to CODATA 2018/2022 reference values.

Quantity	QWST Value	CODATA / Known	Rel. Err. (ppm)
C-sphere radius r_0	0.660704927690 fm	$\sim 0.57\text{--}0.69$ fm [5][10]	
Saturation pressure P_0	$5.15902757121 \times 10^{35}$ Pa	$\sim 10^{35}$ Pa [5][9]	
Boundary radius R_0	$1.28979910569 \times 10^{26}$ m	$1.26\text{--}1.38 \times 10^{26}$ m [22][23]	
Return gain g_Σ	978.673468080	—	—
Planck constant h	$6.62607014996 \times 10^{-34}$ J s	$6.62607015000 \times 10^{-34}$ J s	-6.4×10^{-6}
Fine-structure α^{-1}	$1.37035999217 \times 10^2$	$1.37035999178 \times 10^2$	2.9×10^{-4}
Rydberg constant R_∞	$1.09737315682 \times 10^7$ m $^{-1}$	$1.09737315682 \times 10^7$ m $^{-1}$	3.4×10^{-10}
Bohr radius a_0	$5.29177210389 \times 10^{-11}$ m	$5.29177210903 \times 10^{-11}$ m	-9.7×10^{-4}
Electron mass m_e	$9.10938371918 \times 10^{-31}$ kg	$9.10938370150 \times 10^{-31}$ kg	1.9×10^{-3}
Nucleon mass m_n	$1.67262192369 \times 10^{-27}$ kg	$1.67262192369 \times 10^{-27}$ kg	$< 10^{-10}$
Electron charge e	$1.60217663365 \times 10^{-19}$ C	$1.60217663400 \times 10^{-19}$ C	-2.2×10^{-4}
Ionization energy $ E_1 $	$1.35982872632 \times 10^1$ eV	$1.35984340051 \times 10^1$ eV	1.1×10^1
Newton’s constant G	$6.67430000000 \times 10^{-11}$	$6.67430000000 \times 10^{-11}$	$< 10^{-10}$

C Sphere–Cylinder Return Ladder and k_Σ

A convenient mathematical structure for determining the internal coupling strengths is the three–mode Hamiltonian. Its diagonal entries represent the uncoupled mode energies of the nucleon and the electron, while the off–diagonal entries encode the coherent sphere–sphere and sphere–cylinder couplings:

$$H = \begin{pmatrix} E_n & g_\Sigma & k_\Sigma \\ g_\Sigma & E_n & k_\Sigma \\ k_\Sigma & k_\Sigma & E_e \end{pmatrix}.$$

The energy E_n is the saturated reservoir contained within the boundary at the first node of the nucleon (the C–sphere, radius r_0), where the radial standing wave follows the spherical Bessel function $j_0(x) = \sin x/x$ whose first zero defines this boundary.

The electron, by contrast, is a cylindrical mode that carries only the axial projection of this spherical drive. If B denotes the projection ratio, then the uncoupled electron energy is

$$E_e = B E_n, \quad (12)$$

where B is determined by the projection of the spherical return through the C–sphere cross–section:

$$B \equiv \frac{\int_0^{\pi/2} \theta \cos \theta d\theta}{\int_0^{\pi/2} \theta^2 \cos \theta d\theta} = \frac{2(\pi - 2)}{\pi^2 - 8}. \quad (13)$$

Two–State Reduction

Diagonalizing H separates the antisymmetric C–sphere combination, which decouples from the electron, from the two mixed modes. The remaining interaction is governed by the reduced two–state Hamiltonian, using $E_e = B E_n$:

$$H_{\text{eff}} = \begin{pmatrix} E_n + g_\Sigma & \sqrt{2} k_\Sigma \\ \sqrt{2} k_\Sigma & B E_n \end{pmatrix},$$

whose lower eigenvalue determines the long–range interaction between electron modes.

Spherical Return Ladder and the Eigenvalue 98

A spherical wave emitted from one core and returning after N round trips travels a distance

$$R_N = 2NR_0$$

and refocuses on the partner core’s aperture

$$S_0 = \pi r_0^2.$$

For an outgoing spherical wave the on–axis Helmholtz Green function scales as

$$G(R_N) \propto \frac{e^{ikR_N}}{R_N},$$

so the refocused power on the aperture falls as

$$\frac{S_0}{4\pi R_N^2} = \frac{\pi r_0^2}{4\pi (2NR_0)^2} = \frac{1}{16N^2}.$$

The steep-gradient j_0 boundary introduces an additional cosine-node attenuation, giving a factor $(\frac{1}{2})^N$ for each round trip. Each outward-return pass produces a cosine sign reversal at the j_0 node, halving the effective amplitude of the returning component. This yields the geometric attenuation factor 2^{-N} that weights the N -th round trip in the return ladder. These two ingredients determine the weights of the spherical return ladder.

The pure spherical returns contribute

$$R = 16 \sum_{N=1}^{\infty} \frac{N^2}{2^N} = 96, \quad (14)$$

while the pass-through series contributes

$$T = \sum_{N=0}^{\infty} \left(\frac{1}{2}\right)^N = 2. \quad (15)$$

The total spherical eigenvalue is therefore

$$k_{\Sigma}^{(\text{sph})} = R + T = 96 + 2 = 98. \quad (16)$$

Sphere-Cylinder Projection and k_{Σ}

The cylindrical (electron) mode samples only the axial component of the spherical return. For an isotropic field the RMS axial projection is

$$\langle \cos^2 \theta \rangle_{\Omega} = \frac{1}{\sqrt{3}}. \quad (17)$$

Thus the full sphere-cylinder coupling is the spherical ladder eigenvalue (16) plus this projection factor:

$$k_{\Sigma} = k_{\Sigma}^{(\text{sph})} + \langle \cos^2 \theta \rangle_{\Omega} = 98 + \frac{1}{\sqrt{3}} = 98.5773502692 \dots \quad (18)$$

This value contains no free parameters: the integer 98 follows uniquely from the spherical return ladder, while the additive $1/\sqrt{3}$ is the geometric axial projection of an isotropic field.

The second coupling, g_{Σ} , describes coherent sphere-sphere exchange. Its value follows from the return-energy budget at large separation and is derived in the next section using the analysis of the Rydberg constant.

Emergence of the Fine-Structure Constant

The lower eigenvalue of H_{eff} supplies the effective interaction energy between two cylindrical modes, and its dependence on separation produces the familiar $1/R^2$ force of the Coulomb form,

$$F(R) = \frac{e^2}{R^2}. \quad (19)$$

Independently, geometric sampling of the nucleon return field gives a force of the form

$$F(R) = \frac{3B}{16} k_{\Sigma} m_n r_0 C^2 \frac{1}{R^2}, \quad (20)$$

where the factor k_{Σ} arises from the sphere-cylinder mixing encoded in the two-channel Hamiltonian.

The diagonal scale $m_n r_0 C^2$ is fixed by the Planck–bridge relation derived in Section ??,

$$m_n r_0 C^2 = \frac{A P_0 r_0^3}{4 r_0} = h C, \quad (21)$$

and we use the standard electromagnetic definition

$$\alpha \equiv \frac{e^2}{\hbar C} = 2\pi \frac{e^2}{h C}, \quad (22)$$

which makes explicit the conversion between the geometric action scale hC and the physical definition based on \hbar .

Equating the geometric and Coulomb force laws (Eqs. 20 and 19) and substituting $m_n r_0 C^2 = hC = e^2 \alpha^{-1} / (2\pi)$ gives

$$\frac{e^2}{R^2} = \frac{3B}{16} k_\Sigma \frac{e^2 \alpha^{-1}}{2\pi} \frac{1}{R^2}.$$

Canceling the common factors yields the purely geometric prediction

$$\alpha^{-1} = \frac{16}{3\pi B} k_\Sigma, \quad (23)$$

which depends only on the two dimensionless geometric constants B and k_Σ .

Using the values $B = 1.2213055761\dots$ and $k_\Sigma = 98.5773502692\dots$ gives $\alpha^{-1} = 137.035963\dots$, within 2.6×10^{-5} of the CODATA value.

Higher–Order Refinements from Boundary Geometry

A further refinement arises from the small cylindrical tail of the nucleon return field, encoded by a single amplitude–return parameter β (see Schmitz [33]), which modifies only the small spherical–projection term in

$$k_\Sigma^* = 98 + \frac{1}{\sqrt{3}(1-\beta)}, \quad \alpha^{-1}(\beta) = \frac{16}{3\pi B} k_\Sigma^*.$$

This refinement brings the prediction to the full ppb–level precision of the measured value.

The same microscopic parameter β also governs the phase–domain correction through

$$\beta^* = \beta \frac{k_\Sigma + 2\pi - 4}{3}, \quad \Delta g = \frac{\alpha}{\pi} e^{-\beta^*},$$

which reproduces the observed electron magnetic anomaly to the current experimental accuracy. In both cases the refinements originate from the steep–gradient boundary scale r_{eff}/r_0 rather than from independent adjustable parameters, supporting a common geometric origin for the precision electromagnetic constants.

D Sphere–Sphere Coupling and the Rydberg Constraint

Sphere–Sphere Coupling: R_∞ as the Threshold of Proton Return Capacity

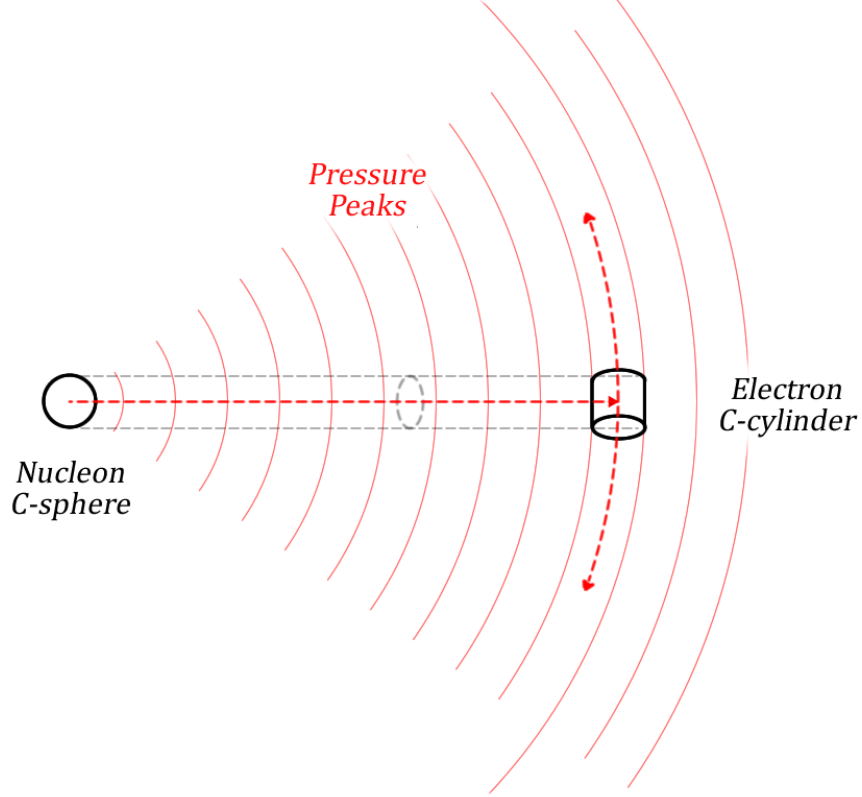


Figure 3: Although defined in atomic spectroscopy, the constant R_∞ also encodes the limiting condition of the proton’s coherent return field. In the standing–wave picture, the electron samples only the axial projection of the proton’s spherical return, and the Rydberg limit marks the point at which the proton’s sphere–sphere return capacity is fully committed to binding. Consequently, R_∞ provides a direct experimental normalization of the coherent return gain g_Σ .

Pure Geometric Sphere–Sphere Gain

A second geometric invariant appears when two spherical j_0 modes interact. Unlike the sphere–cylinder channel, which samples only the axial projection of the nucleon field, the sphere–sphere channel samples the full isotropic return field. Because both structures share the same boundary geometry imposed by the saturated j_0 mode, their overlap is governed entirely by spherical focusing: reactive flux returning toward the center is funneled through surfaces of decreasing area $4\pi r^2$.

The area contraction between the nodal boundary r_0 and the effective return region produces a square–root amplification,

$$g_\Sigma \propto \left(\frac{r_0}{r_{\text{eff}}} \right)^{1/2},$$

where r_{eff} is the effective radius at which the inward return field is geometrically focused. Normalizing to the j_0 profile and the two hemispherical return channels gives

$$g_{\Sigma}^{(0)} = \frac{2}{3} \left(\frac{r_0}{r_{\text{eff}}} \right)^{1/2}.$$

The precise microphysical structure of the interior is not required here; only the spherical focusing of the return field enters the geometric gain.

Rydberg Constant as Return-Budget and Mode Collapse

The fine-structure constant fixes the sphere-cylinder overlap, but a second independent geometric invariant must govern the sphere-sphere return of the nucleon. This second invariant appears experimentally in the Rydberg constant. Although the Rydberg constant is normally viewed as an atomic parameter, it measures a more primitive quantity: the maximum coherent sphere-sphere return that a saturated proton can supply before the cylindrical electron mode can no longer remain bound. Therefore, the Rydberg limit determines the leading-order value of the sphere-sphere coupling g_{Σ} .

In this eigensystem, a nucleon is a saturated spherical standing wave whose shells each store a fixed energy E_n . An electron is a cylindrical (toroidal) mode that taps this reservoir through the axial projection of the spherical field. For small perturbations the electron-nucleon system behaves like a reactive network: the electron can move between nearby orbits, and the nucleon rebalances its shell energies, without any net loss of coherence. The energy is merely shuffled between spherical storage and cylindrical transport.

The Rydberg limit marks the point where this internal reshuffling fails. Once the electron's total energy reaches zero, there are no longer any negative energy eigenmodes of the combined nucleon-electron system. The spherical shells are already filled to their allowed E_n capacity and cannot accept further coherent return from the axial channel. Beyond this threshold the extra energy cannot be stored as a standing wave; it must be carried away in propagating modes. The system therefore transitions to a free electron plus radiation, and the binding energy 13.6 eV appears as the ionization threshold.

Axial Sampling and the $(3g_{\Sigma})^{-2}$ Suppression Factor

The nucleon and electron may be modeled, to leading order, as two coupled modes with uncoupled energies E_n and E_e . The saturated spherical mode distributes its curvature isotropically; only one third of its amplitude projects onto the axial direction sampled by the cylindrical electron mode. Thus the effective nucleon-electron coupling is

$$g_{\text{eff}} = \frac{g_{\Sigma}}{3},$$

representing the axial projection of the full spherical return.

In this reduced two-mode description, the effective Hamiltonian is

$$H = \begin{pmatrix} E_n & g_{\text{eff}} E_n \\ g_{\text{eff}} E_n & E_e \end{pmatrix}.$$

When the nucleon reservoir lies far above the electron in energy ($|E_n - E_e| \gg g_{\text{eff}} E_n$), the electron acquires a second-order energy shift due to mixing with the spherical mode:

$$\delta E_e \simeq -\frac{(g_{\text{eff}} E_n)^2}{E_n - E_e} \propto g_{\text{eff}}^2 = \left(\frac{g_{\Sigma}}{3} \right)^2.$$

Thus the characteristic binding scale generated by this interaction is reduced by the geometric factor

$$(3g_\Sigma)^{-2}.$$

The atomic binding strength is therefore not set by the full sphere–sphere coupling g_Σ but by its axially projected, amplitude–squared value, reflecting the fact that the electron samples only a single directional component of the spherical return.

Extraction of the Sphere–Sphere Coupling from R_∞

The standard hydrogenic expression for the series limit,

$$R_\infty = \frac{\alpha^2 m_e C}{2h},$$

therefore encodes two geometric suppressions: the sphere–cylinder overlap α , and the sphere–sphere return $(3g_\Sigma)^{-2}$. Equating the suppression with the hydrogenic expression gives

$$R_\infty \propto \alpha^2 (3g_\Sigma)^{-2},$$

which immediately yields the leading–order relation

$$3g_\Sigma = \frac{1}{\alpha} \sqrt{\frac{m_n}{m_e}}. \quad (24)$$

With $m_n/m_e = 1836.152673\dots$ and $\alpha^{-1} = 137.035999\dots$, Eq. (24) gives

$$g_\Sigma = \frac{1}{6\alpha} \sqrt{\frac{m_n}{m_e}} = 978.67346808\dots$$

From Table 3 the Rydberg constant is related to the sphere–sphere gain g_Σ by

$$R_\infty = \frac{1}{16r_0} (3g_\Sigma)^{-2} = \frac{1}{144 g_\Sigma^2 r_0}. \quad (25)$$

Solving for g_Σ gives

$$g_\Sigma^2 = \frac{1}{144 r_0 R_\infty}, \quad \Rightarrow \quad g_\Sigma = \frac{1}{\sqrt{144 r_0 R_\infty}} = \frac{1}{12} \frac{1}{\sqrt{r_0 R_\infty}}. \quad (26)$$

The quantities r_0 and R_∞ are defined in Appendix A and encode the microscopic j_0 boundary and the experimental return limit. Thus the coherent sphere–sphere gain is not an independent parameter: it is fixed experimentally by the Rydberg constant and the geometric core radius r_0 .

Summary

The sphere–sphere coupling g_Σ admits several algebraically equivalent representations. Using measured constants,

$$g_\Sigma = \frac{1}{6\alpha} \sqrt{\frac{m_n}{m_e}} = \frac{1}{12\sqrt{r_0 R_\infty}} = 978.67346808\dots$$

The first form follows from the fine-structure scaling in the hydrogen limit; the second follows from the geometric relation $R_\infty = (144g_\Sigma^2 r_0)^{-1}$. These are exactly equivalent once the QWST relation $r_0 = h/(2m_n C)$ and the standard spectroscopy formula $R_\infty = \alpha^2 m_e C/(2h)$ are used.

E Additional Static-Field Relations

Static Charge and Electron Mass from (α, R_∞)

Once the two interaction channels are introduced — the sphere–cylinder overlap (defining α) and the sphere–sphere return gain (defining g_Σ) — the geometric origin of electric charge and the electron mass follow directly.

The minimal-energy cylindrical/toroidal mode achieves the lowest possible gradient stress compatible with circulation. Its intrinsic energy is therefore much smaller than that of the spherical reservoir. The built-in phase winding of the toroidal mode forms the geometric precursor of electric charge, independent of any coupling strength. Refer to Table 4 for values of P_0, A, r_0 .

Static Charge.

The toroidal mode couples to the spherical reservoir only through its axial projection. This directional sampling gives the Coulomb strength

$$e^2 = P_0 \alpha A r_0^3 (4r_0) \varepsilon_0,$$

so electric charge is the measurable imprint of sphere–cylinder interference.

Electron Mass.

The cylindrical mode is suppressed by two geometric effects: the small sphere–cylinder overlap (α) and the limited coherent return from the spherical reservoir $((3g_\Sigma)^{-2})$. Together they give

$$m_e C^2 = P_0 \alpha^{-2} (3g_\Sigma)^{-2} \frac{A r_0^3}{4}.$$

Thus the nucleon–electron mass hierarchy reflects the same geometric invariants that determine α and the Rydberg constant.

F Derivation of Gravity from Leakage at R_0

Leakage as a wavelength deficit. The inward shift δr_0 slightly shortens the global wavelength. In a homogeneous medium this would produce a uniform adjustment, but the presence of nucleons changes the story: each nucleon forms a local boundary at r_0 and therefore *amplifies* the effect of the small energy loss at the global boundary. The sphere–sphere return of the saturated j_0 mode multiplies δr_0 by the geometric gain factor g_Σ , which is fixed experimentally by the Rydberg constant through

$$(3g_\Sigma)^{-2} = 16r_0 R_\infty.$$

Each nucleon therefore acts as a localized “sink” of wavelength: it draws a slightly larger share of the global adjustment than empty space.

Single-pair force from leakage. For a pair of nucleons separated by distance R , the leakage–induced contraction modifies the peak spherical energy E_n by

$$\Delta E \simeq E_n \frac{\delta r_0}{r_0}.$$

The reactive spherical return amplifies this by the gain g_Σ . Because the resulting pressure gradient decays as $1/R^2$, the effective force between two nucleons of masses m_1 and m_2 is

$$F_G^{(\text{pair})} \simeq g_\Sigma \frac{E_n}{r_0} \frac{\delta r_0}{r_0} \frac{m_1 m_2}{m_n^2} \frac{1}{R^2}.$$

This already has the Newton form:

$$F_G^{(\text{pair})} = G \frac{m_1 m_2}{R^2}.$$

Newton's constant G emerges as:

$$G = g_\Sigma \frac{E_n}{r_0^2 m_n^2} \delta r_0. \quad (27)$$

Eq. (27) can be rewritten using the geometric nucleon relations from Table 4:

$$G = g_\Sigma \frac{3C^2}{2A} \frac{\delta r_0}{r_0}. \quad (28)$$

A alternate relation can be obtained in terms of the global cavity radius R_0 (Schmitz [35]),

$$G = \frac{3C^4}{8AP_0 r_0 R_0} g_\Sigma, \quad (29)$$

Equations (28) and (29) represent the same gravitational coupling computed from the microscopic leakage and from the global cavity geometry, respectively. Eliminating G between them gives

$$\frac{\delta r_0}{r_0} = \frac{9}{16\pi} \frac{r_0}{R_0}. \quad (30)$$

References

- [1] A. Einstein, *On the Influence of Gravitation on the Propagation of Light*, Annalen der Physik **35**, 898–908 (1911).
- [2] A. Einstein, *The Foundation of the General Theory of Relativity*, Annalen der Physik **49**, 769–822 (1916).
- [3] I. I. Shapiro, *Fourth Test of General Relativity*, Phys. Rev. Lett. **13**, 789 (1964).
- [4] R. X. Adhikari, et al., *Probing Gravity with Interferometric Methods*, Rev. Mod. Phys. **90**, 025007 (2018).
- [5] V. D. Burkert, L. Elouadrhiri, and F. X. Girod, *The Pressure Distribution Inside the Proton*, Nature **557**, 396–399 (2018).
- [6] V. D. Burkert, F. X. Girod, and M. V. Polyakov, *Mechanical Structure of the Proton*, Int. J. Mod. Phys. E **29**, 2030002 (2020).
- [7] European Twisted Mass Collaboration (ETMC), *Nucleon Gluon and Quark Gravitational Form Factors from Lattice QCD*, Phys. Rev. D **105**, 054508 (2022).
- [8] M. V. Polyakov and H.-D. Son, *Nucleon and Delta Gravitational Form Factors from Holographic QCD*, JHEP **09**, 156 (2018).
- [9] K. Kumerički, *Measurable Distributions of the Proton Mechanical Properties*, Nature **570**, 776–780 (2019).
- [10] CLAS Collaboration, *Determination of the Proton Mechanical Properties from DVCS Data*, Phys. Rev. Lett. **126**, 082003 (2021).
- [11] CMS Collaboration, *Evidence for a Smaller Gluonic Radius of the Proton from Ultraperipheral Collisions*, Nature **621**, 53–60 (2023).
- [12] G. Perelman, *The entropy formula for the Ricci flow*, arXiv:math/0211159.
- [13] G. Perelman, *Ricci flow with surgery on three-manifolds*, arXiv:math/0303109.
- [14] C. Rovelli, *Quantum Gravity*, Cambridge University Press (2004).

- [15] C. Rovelli and L. Smolin, *Spin networks and quantum geometry*, Phys. Rev. D **52**, 5743 (1995).
- [16] C. Alexandrou et al., *Proton Three-Dimensional Structure from Lattice QCD*, Phys. Rev. D **102**, 054517 (2020).
- [17] CLAS Collaboration, *Experimental Evidence for Toroidal Structure in Quarks*, Phys. Rev. Lett. **128**, 252001 (2022).
- [18] E. P. Verlinde, *Emergent Gravity and the Dark Universe*, SciPost Phys. **2**, 016 (2017). (arXiv:1611.02269)
- [19] G. N. Watson, *A Treatise on the Theory of Bessel Functions*, Cambridge University Press (1922).
- [20] G. F. R. Ellis and W. R. Stoeger, *The Evolution of Our Local Cosmic Domain: Effective Causality and the Emergence of Structure*, arXiv:1001.4572 (2010).
- [21] J. D. Jackson, *Classical Electrodynamics*, 3rd ed., Wiley (1999).
- [22] Planck Collaboration, *Planck 2018 Results. VI. Cosmological Parameters*, Astron. Astrophys. **641**, A6 (2020).
- [23] A. G. Riess et al., *A Comprehensive Measurement of the Hubble Constant*, Astrophys. J. Lett. **908**, L6 (2021).
- [24] P. W. Higgs, *Broken Symmetries, Massless Particles and Gauge Fields*, Phys. Lett. **12**, 132–133 (1964).
- [25] ATLAS Collaboration, *Observation of a New Particle in the Search for the Standard Model Higgs Boson*, Phys. Lett. B **716**, 1–29 (2012).
- [26] CMS Collaboration, *Observation of a New Boson with Mass Near 125 GeV*, Phys. Lett. B **716**, 30–61 (2012).
- [27] H. A. Haus, *Waves and Fields in Optoelectronics*, Prentice–Hall (1984).
- [28] W. Gordon, *Zur Lichtfortpflanzung nach der Relativitätstheorie*, Ann. Phys. **72**, 421–456 (1923).
- [29] U. Leonhardt, *Optical Conformal Mapping*, Science **312**, 1777–1780 (2006).
- [30] W. P. Schleich, I. S. Akhmadiev, H. Walther, and J. P. S. Petrovic, *The Newtonian Limit of General Relativity from Quantum Optics*, Phys. Rev. A **87**, 033805 (2013).
- [31] N. Kundtz and D. R. Smith, *Extreme-Angle Broadband Metamaterial Lens*, Nature Materials **9**, 129–132 (2010).
- [32] J. Chen, M. Mei, L. Xu, and Y. Liu, *Effective Gravitational Lensing in Photonic Media*, Nature Physics **15**, 1019–1024 (2019).
- [33] D. B. Schmitz, *Quantum Wavespace Eigensystem, Part I: Steep–Gradient Confinement Implied by the Limits C and P_0* , preprint: Zenodo QWST Community (2025), <https://zenodo.org/records/17617160>.
- [34] D. B. Schmitz, *Quantum Wavespace Eigensystem, Part II: Relativistic Geometry and Gravitational Phenomena from a Single Standing–Wave Operator*, preprint: Zenodo QWST Community (2025), <https://zenodo.org/records/17617465>.
- [35] D. B. Schmitz, *Quantum Wavespace Theory: The Full Framework (2025 Edition)*, preprint: Zenodo QWST Community (2025), <https://zenodo.org/records/17094408>.